# Active Vibration Control of a Smart Fin

Fatma Demet Ulker *
*Ottawa, ON, K1S5B6, CANADA*

Volkan Nalbantoglu †
*Ankara, 06531, TURKEY*

Yong Chen ‡ and David Zimcik §
*Ottawa, ON, K1A0R6, CANADA*

Yavuz Yaman ¶
*Ankara, 06531, TURKEY*

**This paper summarizes the design and wind tunnel experimental verifications of robust $H_\infty$ controllers for active vibration suppression of a dynamically scaled F-18 vertical smart fin. The smart fin consists of a cantilevered aluminium plate structure with surface bonded piezoelectric (Lead-Zirconate-Titanete, PZT) patches, Integrated Circuit Piezoelectric (ICP) type accelerometers and strain gauges. For $H_\infty$ controller design, the transfer function of the fin was first estimated outside the wind tunnel. Then, experiments were carried out to determine the aeroelastic characteristics of the smart fin at free flow and vortical (i.e. buffet) flow conditions. Variable air speeds and Angle of Orientations (AoO) were considered in both flow conditions. Significant shifts in vibration frequencies and the damping ratios were observed at the various values of airspeed and AoO. Taking into account these variations, the $H_\infty$ controllers were designed to suppress the fin's buffeting response at the first and second bending and first torsional modes. A second set of wind tunnel experiments was conducted to verify the performance of the designed $H_\infty$ controllers at various flow scenarios. Successful vibration suppression levels were obtained within the desired frequency intervals.**

## I. Introduction

VERTICAL fins of high performance aircraft conducting high angle of attack maneuvers are often subjected to high buffet loading due to vortices emanating from wing/fuselage leading edge extensions (LEX).[1] The resultant vibrations increase the risk of structural fatigue failure. To prevent this undesirable outcome, there has been a great deal of research in this area.[1–6] A majority of the methods proposed feature either alteration of the flow field around the vertical fin, structural modification of the fin and/or active control. For example, active control of the fin using surface bonded PZT patches/fiber actuators[1–3] and an actively controlled rudder[4,5] have been studied. Effectiveness of the different control strategies were investigated using ground vibration test and wind tunnel experiments. Regarding the control of flow around the fin, several techniques have been applied to change either the position of the vortex with respect to the fin or delay vortex breakdown with blowing, suction on the wing surface, addition of fences, and variable position leading-edge extensions.[6]

The work summarized in this paper is the second and final part of a two part project lead by Middle East Technical University (METU). The first part of the research project dealt with the design of the scaled fin and the determination of optimal actuator/sensor placement locations using Finite Element Methods (FEM).[7] Moreover, theoretical and experimental verification of the actively controlled smart fin under free/forced in-vacua vibrations using $H_\infty$ and $\mu$ robust control design techniques was completed.[8,9] Finally, flutter control analysis was performed using MSC/NASTRAN.[10]

The aim of the present research was to design and experimentally validate the effectiveness of $H_\infty$ robust controllers for vibration suppression of the smart fin under various types of aerodynamic loads. First, the system model of the smart fin was obtained through open loop experiments at no-flow condition. The

*PhD Candidate, Department of Mechanical and Aerospace Engineering, Carleton University
†Dr., Department of Aerospace Engineering, Middle East Technical University
‡Dr., Institute for Aerospace Research, National Research Council Canada
§Dr., Institute for Aerospace Research, National Research Council Canada
¶Prof., Department of Aerospace Engineering, Middle East Technical University

influence of aeroelastic coupling and higher order mode truncation on the system model was introduced as parametric and additive uncertainty in the $H_\infty$ controller design. Wind tunnel experiments were carried out in the low speed wind tunnel at the Institute for Aerospace Research of the National Research Council Canada (NRCC). Different control strategies were applied to analyze the closed loop vibration characteristics of the smart fin at various free stream wind speeds, orientation angles and the effect of additional aerodynamic loading from a Kalman Vortex generator located upstream of the smart fin.

## II. Smart Fin

The dynamics of the fin structure was designed to simulate the first two bending and first torsional modes of the F-18 vertical fin in a clamped-free configuration. The smart fin was constructed by symmetrically attaching twenty-four PZT patches ($25mm \times 25mm \times 0.5mm$, SensorTech BM500 type) as actuators and six strain gauges (OMEGA-SG-7/350-LY13) and ICP type accelerometers as sensors on a passive aluminum plate-like structure called the fin. The actuators and sensors were placed at determined locations having high strain/displacement as a result of previous finite element analysis.[7] However, in the present study only the accelerometers located at the aft-fin-tip and leading edge of the smart fin as shown in Figure 1 were utilized.

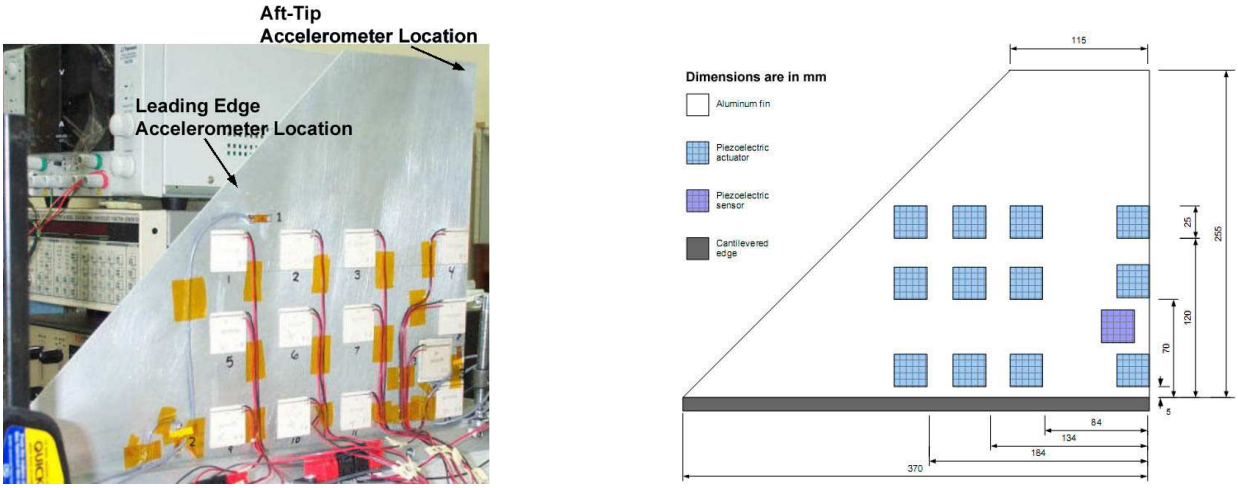


(a) Photo

(b) Schematic View

**Figure 1. Smart Fin Used in the Study**

The PZT patches were insulated from the aluminum plate to increase controller design flexibility. For the various controller implementations, the PZT patches were used in groups. *Group* 1 includes the eight PZT patches in the $1^{st}$ and $2^{nd}$ rows from fin tip on both sides. *Group* 2 includes the bottom row PZT patches on both sides. Finally, *Group* 3 includes all the PZT patches on each side. PZT patches on the front face and back face of the fin were operated with opposite phase. Figure 2 illustrates the PZT patch grouping.

### A. Structural Model of Smart Fin

The FEM results were validated using experimental modal analysis using the LMS Test.Lab Modal Analysis package. The smart fin was excited with a base shaker within the frequency range $0.1Hz$ to $150Hz$. Vibrations of the smart fin were measured at the nodal grid points using ICP type accelerometers. Comparison of experimental and FEM $1^{st}$ bending mode shape of the smart fin is shown in Figure 3.

### B. Aeroelastic Response of Smart Fin

Under aerodynamic loading, the system characteristics will change due to aeroelastic coupling. The effect of aerodynamic loading on the smart fin can be interpreted as an effective additional mass, stiffness and damping; all of which are determined by the flow conditions. The resultant aeroelastic system can be

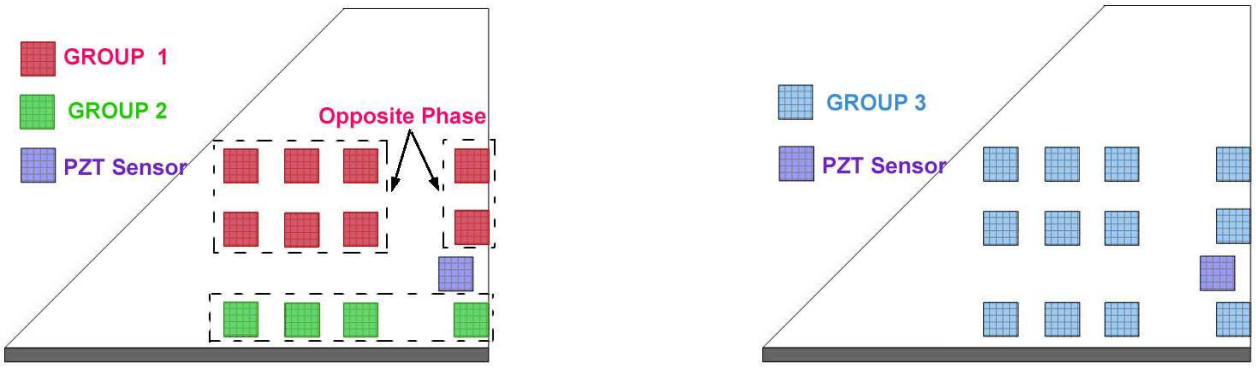


(a) *Group* 1 and 2 (b) *Group* 3

**Figure 2. Smart Fin PZT Patch Groups For Controller Implementation**

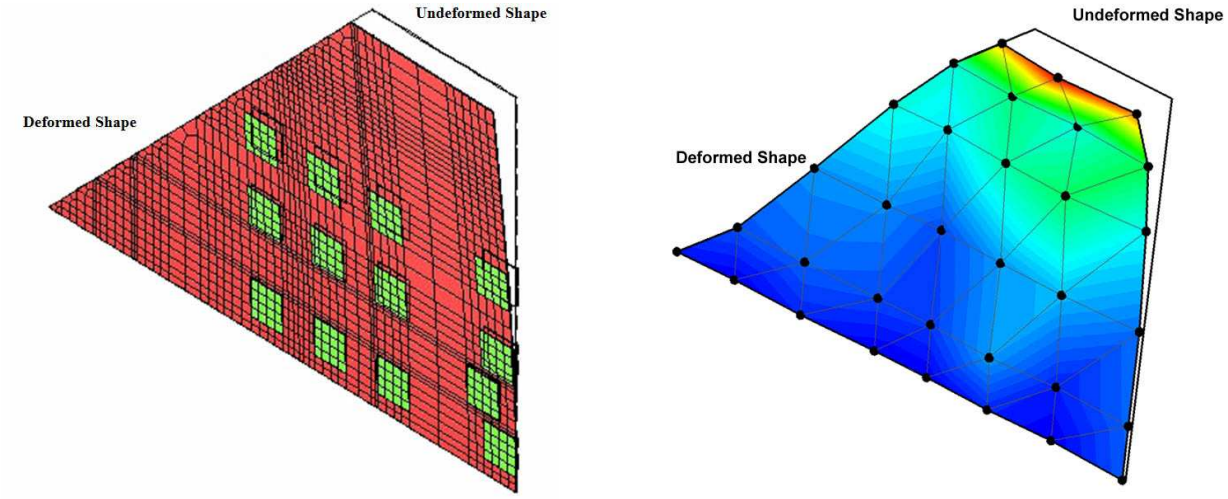


(a) FEM $1^{st}$ Bending Mode Shape (b) Experimental $1^{st}$ Bending Mode Shape

**Figure 3. Comparison of Experimental and FEM $1^{st}$ Bending Mode**

described by the following equation where subscript $s$, $a$ and $e$ stand for structure, aerodynamic and external respectively; $x$ is the state of the system.

$$M_s\ddot{x}(t) + C_s\dot{x}(t) + K_s x(t) = M_a\ddot{x}(t) + C_a\dot{x}(t) + K_a x(t) + F_e(t) \tag{1}$$

or alternatively

$$(M_s - M_a)\ddot{x}(t) + (C_s - C_a)\dot{x}(t) + (K_s - K_a)x(t) = F_e(t) \tag{2}$$

where $F_e$ is the control force from the PZT patches and/or any extraneous aerodynamic loading such as that created by the vortex generator.

For the aeroelastic analysis, the smart fin was subjected to air flows at $0^o$ and $10^o$ angle of orientation (AoO) for two cases called free stream and vortical flow. For free stream airflows, the wind speed was set to range from $10m/s, 20m/s, 30m/s, 40m/s, 45m/s$, which is the maximum operational speed of the NRCC wind tunnel. Vortical flow was generated by locating a square $0.1m$ by $0.1m$ column $1.2m$ upstream of the fin. Due to the strong energy contained in the vortical airflows, the model was tested at airflow speeds of $10m/s, 13m/s$ and $15m/s$ to prevent the PZT ceramic actuators from fracturing. The accelerometers attached to the aft-fin-tip and the leading edge of the smart fin were used as sensors, however for the sake

of brevity only the frequency response plots obtained from the accelerometer located at the aft-fin-tip are presented. The wind tunnel experimental set up is illustrated in Figure 4.

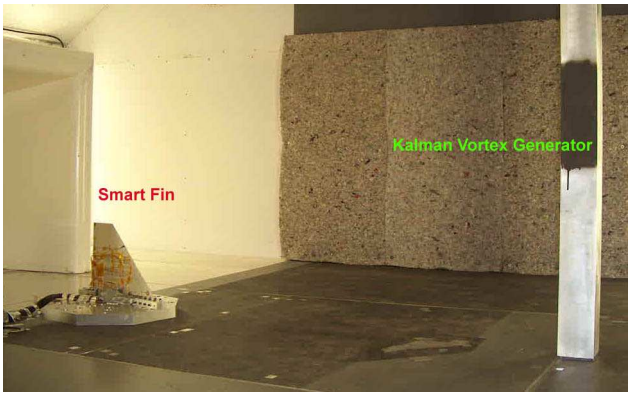


**Figure 4. Wind Tunnel Experimental Setup**

Under the described flow scenarios, wind tunnel experiments were carried out to determine the aeroelastic characteristic of the smart fin. In Figure 5(a), frequency response plots of the smart fin at $AoO = 0^o$ are shown. The shift in frequency and damping ratios are compared with the previously performed flutter analysis of the identical smart fin using MSC/NASTRAN.[10] The root locus graph is shown as a function of flight speed in Figure 5(b) for inflow velocities of $V = 20, 30, \cdots, 90m/s$.

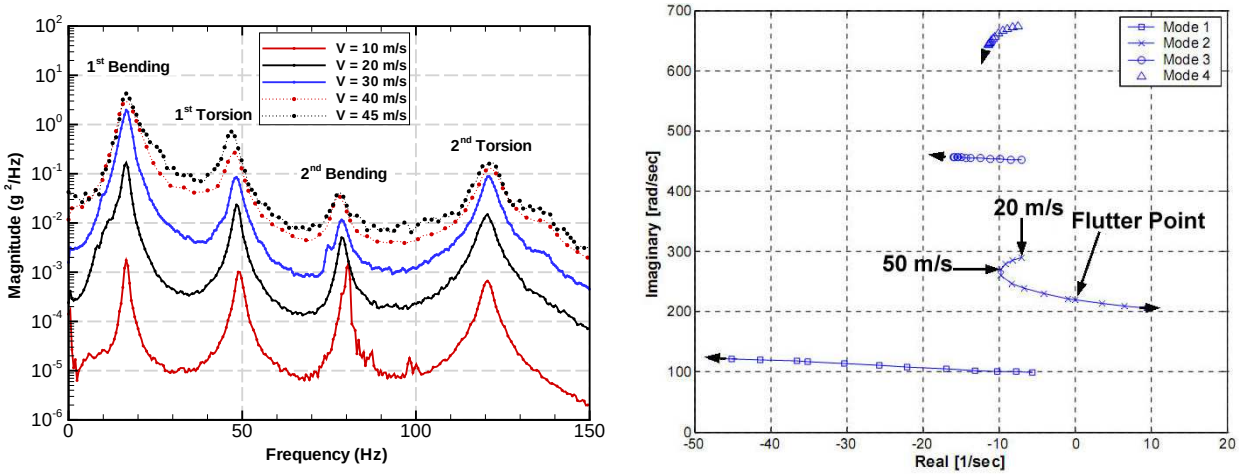


(a) Free Stream Flow $AoO = 0^o$

(b) Root-locus as Function of the Flight Speed[10]

**Figure 5. Fin-aft-tip Frequency Response Plots Under Free Stream Flow**

As seen from the frequency response plots, with increase in air speed, there is considerable increase in the amplitude of vibration at all frequencies. While damping of the modes increased, the modal frequencies of the first torsion and second bending modes shift. The decrease in the first torsional mode frequency was also determined from the previously performed flutter analysis. In Figure 6(a), comparison of frequency response under varying airspeeds is given for $AoO = 0^o$ and $AoO = 10^o$. For $AoO = 10^o$ the shift in frequencies became more significant especially at the higher modes. The details of the modal parameter variation with airflow speed are listed in Table 1.

An identical set of experiments were repeated for the vortical flow condition with an airspeeds of $10m/s$, $13m/s$ and $15m/s$. The comparison in the frequency response plots for $AoO = 0^o$ and $AoO = 10^o$ is given in Figure 6(b).

The peak buffeting frequency of the vortical airflow was $9.8Hz$ at $10m/s$ and increased to $12.9Hz$ at $15m/s$. Although the smart fin was only tested with a relatively small airflow speed range, the measured

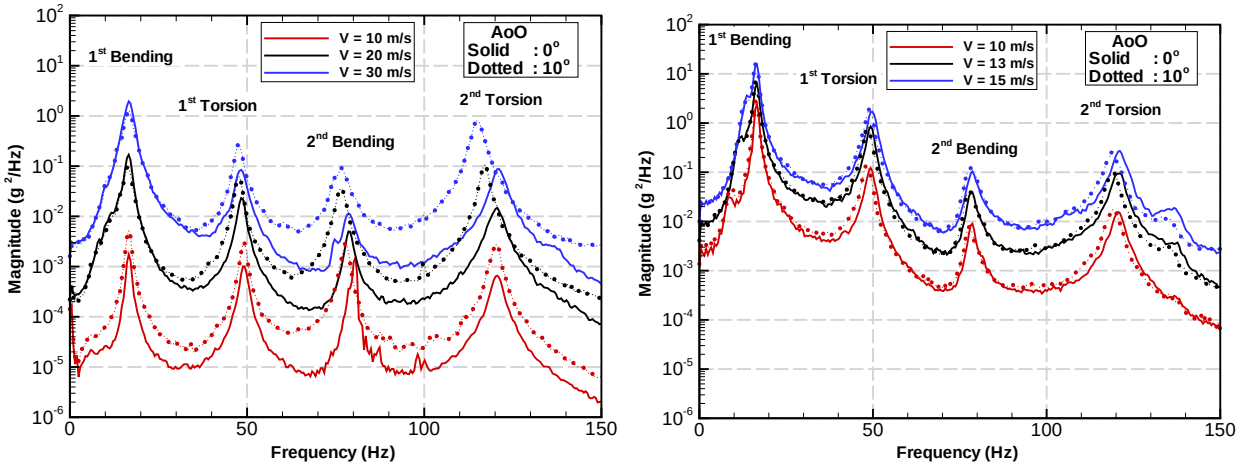


(a) Free Stream Flow $AoO = 0^o$and$AoO = 10^o$

(b) Vortical Flow $AoO = 0^o$and$AoO = 10^o$

**Figure 6. Fin-aft-tip Frequency Response Plots Under Free Stream and Vortical Flow**

vibration level of the $1^{st}$ bending mode at $10m/s$ was comparable to the vibration level measured at $45m/s$ in the free flow air speed case. Also, the variation of modal frequency was substantial because the vortical airflow contained higher buffeting energy compared to the free airflow at the same airflow speed. Similar to the case of free stream airflow, the increased air flow speed introduced higher aerodynamic damping to the smart fin modes. The modal frequencies of the smart fin also decreased with the increase of $AoO$ from $0^o$ to $10^o$ and the effect was more significant to the high vibration modes. The details of the modal parameter variation with airflow speed are listed in Table 2.

## III. System Identification

For the purpose of controller design, the system is assumed to be Linear Time Invariant (LTI). Both Single-Input Multi-Output (SIMO) and Multi-Input Multi-Output (MIMO) system models were analyzed using the PZT patch group definition given in Figure 2. The SIMO model used a single input to *Group* 3 PZT patches, while in the MIMO model, both *Group* 1 and *Group* 2 PZT patches were used as actuators. With the LTI system assumption, the transfer functions from the each PZT patch *Groups* 1, 2, 3 were obtained individually through experiments without aerodynamic disturbances. Three sets of experiments were performed applying sine sweep signal of frequency range 0 to $100Hz$ at a rate of $1.5Hz/s$ to each actuator group. This frequency range was selected to cover the three major vibration modes; the higher vibration modes beyond $100Hz$ including the second torsional mode at $120Hz$ were ignored. The mathematical model of the smart fin was obtained by first applying non-parametric system identification techniques on the open-loop data and then fitting a state-space model to the resulting frequency response functions considering only the first 3 modes. This approach was repeated for each acceleration data set in order to construct the SIMO transfer functions. The resultant state space model has an order of 22 for the SIMO system and 28 for the MIMO system. The scaled estimated transfer functions for the MIMO system are given in Figure 7.

## IV. Controller Design

The objective of feedback control is not only to provide internal stability, but also to achieve certain performance specifications. However, while trying to attain these goals, two drawbacks come into the picture: uncertainty of the system model and measurement errors. As a result of studies in the early 1980s, formulations of a tractable mathematical notion of uncertainty and rigorous mathematical techniques to cope with the uncertainty problems were introduced into the classical control theory.[11,12]

In the present analysis, there are two types of uncertainties which need to be included in controller design. The first is an additive uncertainty ($W_{add}$) which accounts for the unmodeled higher order modes and modeling errors at very low frequencies. The second is the parametric uncertainty due to system

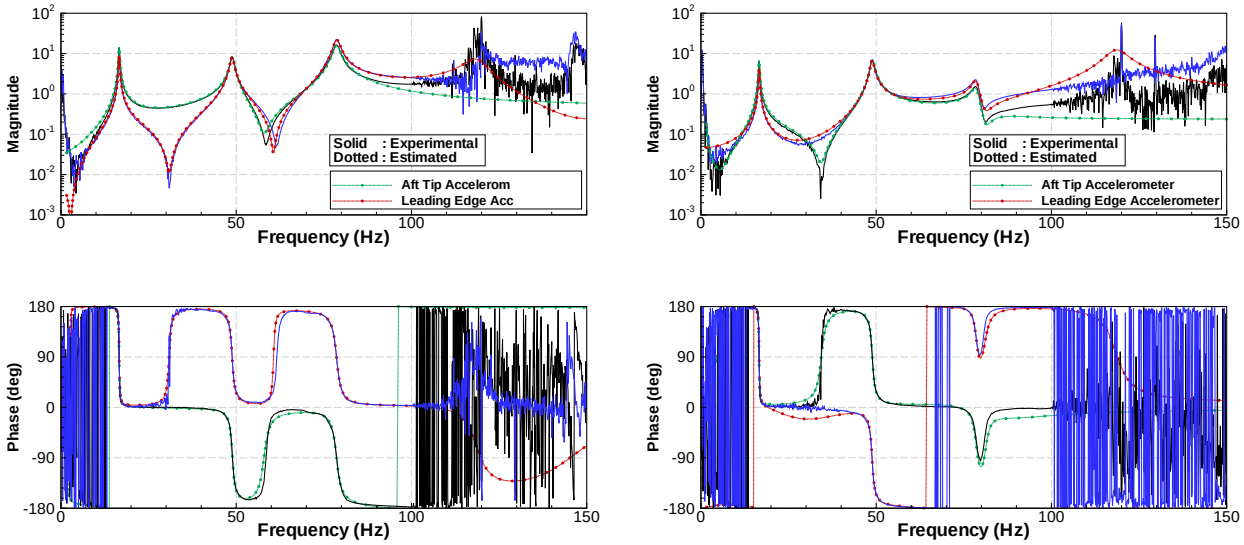


(a) *Group* 1 (b) *Group* 2

**Figure 7. Estimated Transfer Function**

parameter variations $(\delta m, \delta c, \delta k)$ as a result of aeroelastic coupling.

The $H_\infty$ control problem is illustrated in Figure 8. In this diagram, $(SYS_{nom})$ shows the nominal identified model, whose stiffness and damping terms of the first 2 modes are assumed to have 5% parametric uncertainties. Performance weight $(W_{per})$ was selected so that only the vibration due to the first 3 modes was taken into account. $W_{act}$ defines the actuator weight which was selected to limit the output of the controller to $5V_{peak}$, and its frequency variation was ignored.

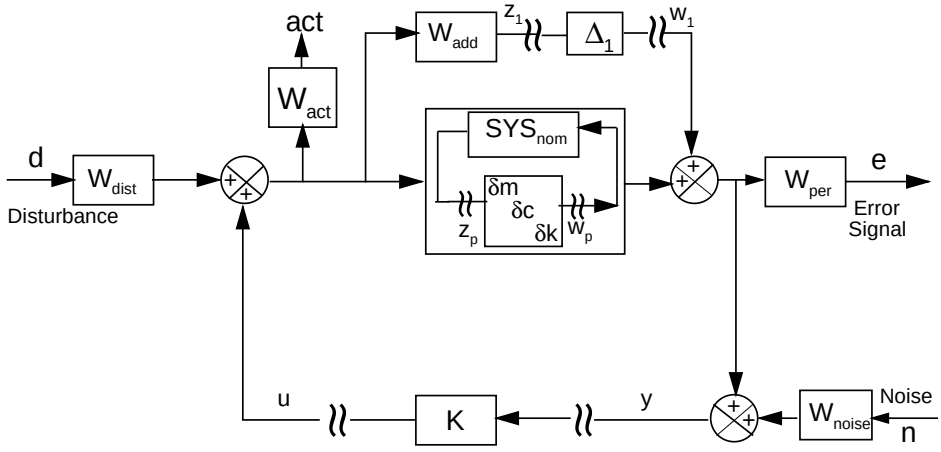


**Figure 8. General Feedback Block Diagram Representation**

On the estimated nominal SIMO and MIMO system models which include the above mentioned uncertainties, $H_\infty$ controllers were designed and robustness analysis were performed. The resultant controller orders were 14 and 16 respectively. An example of selected weights for controller design and robustness tests for the mentioned controllers are presented in Figure 9 and Figure 10 respectively.

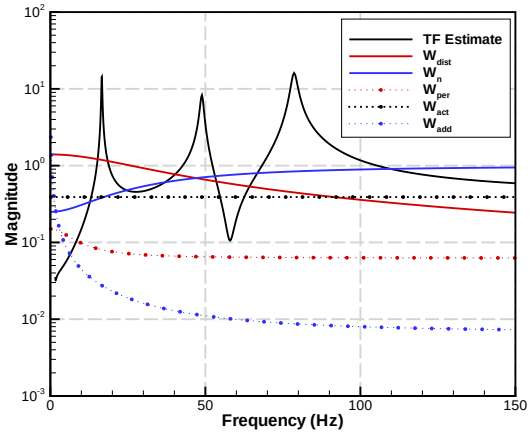


**Figure 9. Controller Design Weights**

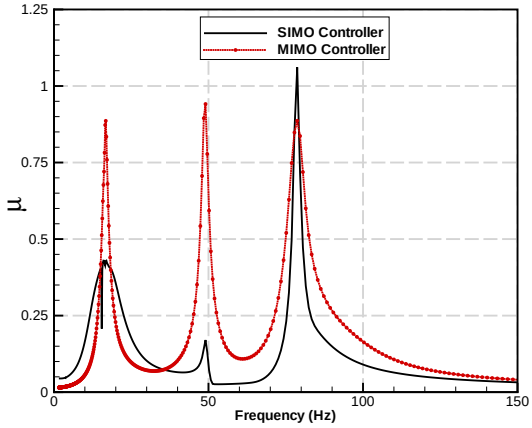


**Figure 10. Robustness Analysis**

According to robustness analysis, both the SIMO and MIMO controllers are predicted to provide good performance levels at the first bending and first torsional modes within the defined uncertainty definitions. However, it is obvious that at second bending mode, the controllers could potentially excite the system. Also, the SIMO controller is not capable of suppressing the first torsional mode, which is an expected result since the SIMO controller uses *Group* 3 PZT patches favoring to excite the bending modes.

Finally, the designed controllers were tested in the wind tunnel at the various flow scenarios mentioned earlier. The following section summarized the closed loop wind tunnel experimental results.

## V. Closed Loop Wind Tunnel Experiments

Closed loop experiments were carried out to determine the performance of the designed controllers and the selected actuator pairs. MATLAB xPC TargetBox platform was used for the implementation of the controllers. The executable code was generated from the Simulink block diagram directly and then transferred to the target computer to run in real-time mode. A sampling rate of 1000Hz was used in the implementation. The calculated control outputs were applied to the two PZT actuator groups through the TREK 50/750 power amplifier.

Figure 11(a) and 11(b) show the Open Loop (OL) and Closed Loop (CL) frequency response plots at different free flow speeds with $AoO = 0^o$ and $AoO = 10^o$ respectively. The comparison of different actuator grouping is also presented for this case as *Group* 3 control, and *Group* 1 and 2 control.

As shown in Figure 11, the $H_\infty$ controller demonstrates effective vibration reduction at all three targeted vibration modes. At the airflow speed of $10m/s$, the reduction achieved at first bending mode, first torsional mode and second bending mode using *Group* 1 and 2 actuators was $18dB$ , $15dB$ and $30dB$ respectively. With the airflow speed increased to $30m/s$, the achieved suppression reduced slightly to $10dB$, $11dB$ and $6.5dB$ due to the limited capacity of excitation provided by the actuators. As seen from the figure, the *Group* 3 actuator can suppress vibrations effectively at the first bending mode but it can not provide twisting excitation to suppress the torsional modes. No obvious control spillover was observed beyond $100Hz$ at either 0 or 10 degree of *AoO* configurations. This shows that, with the proper actuator selection, the designed $H_\infty$ controllers were effective to alleviate the smart fin's vibration caused by the aerodynamic disturbance. Moreover, the proposed control law development strategy is able to account for the unmodeled smart fin dynamics beyond $100Hz$ as well as the modal frequency shift and variation of smart fin damping due to aeroelastic coupling.

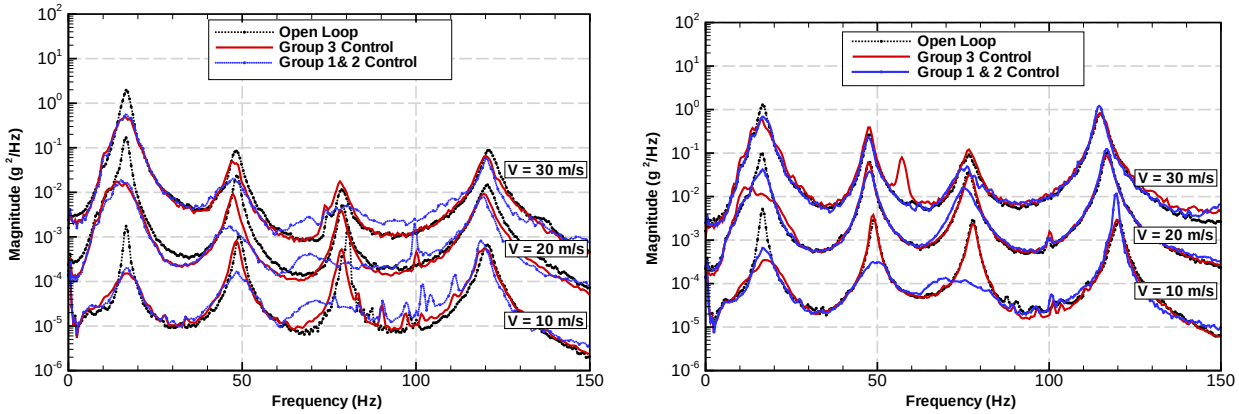


(a) $AoO = 0^o$ (b) $AoO = 10^o$

**Figure 11. Open Loop and Closed Loop Frequency Response Plots of Smart Fin Under Free Stream Flow**

Figures 12(a) and 12(b) show Open Loop (OL) and Closed Loop (CL) frequency response plots for $10m/s$ and $15m/s$ air speed vortical flow condition with $AoO = 0^o$ and $AoO = 10^o$ respectively. The comparison of different actuator grouping is also presented for this case as *Group* 3 control, and *Group* 1 and 2 control.

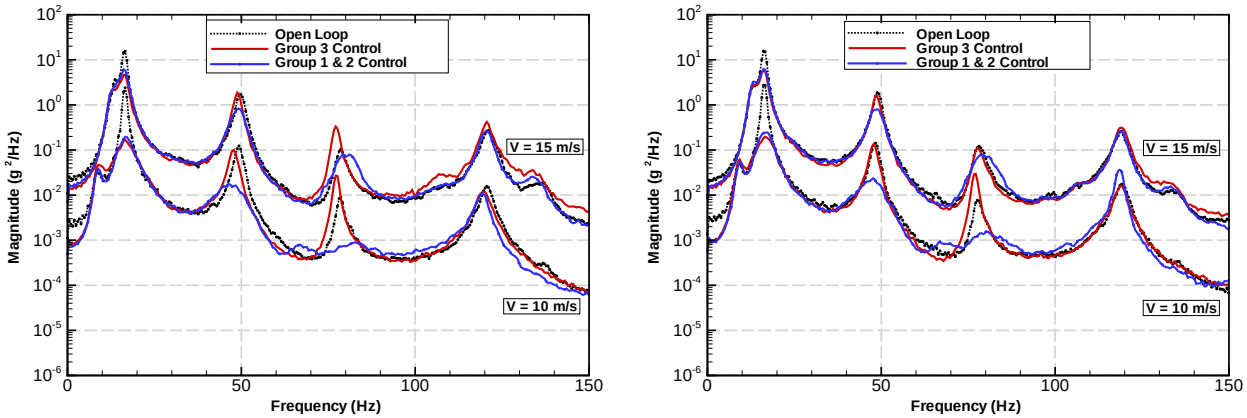


(a) $AoO = 0^o$ (b) $AoO = 10^o$

**Figure 12. Open Loop and Closed Loop Frequency Response Plots of Smart Fin Under The Vortical Flow**

With the increase of air speed the achieved vibration suppression to the three targeted smart fin modes decreased due to the intense buffeting energy resulting from the vortical airflows. At an $AoO$ of 10 degrees and airflow speed of $10m/s$, the first bending mode was suppressed by $16.2dB$, the first torsional mode was suppressed by $4.3dB$ and the second bending mode was reduced by 19.7dB. At an air speed of $15m/s$, suppression to the three vibration modes reduced to 7.2, 5.0 and $8.3dB$ respectively. No obvious control spillover was observed throughout the experiment. To further verify the control law performance, varying air speed condition was generated in the wind tunnel. This was achieved by adjusting the rotating speed of the main motor manually through the console. During the test, the wind tunnel airflow speed was slowly ramped up from 0 to $30m/s$, and then ramped down to $0m/s$ within approximately 90 seconds. Due to the broad speed range, the vortex generator was not used to avoid excessive responses of the smart fin. The control law was kept on throughout the test process. Effective and consistent suppression of smart fin vibration responses were obtained. Typical OL/CL results are shown in Figure 13 as waterfall plots.

By comparing the two waterfall plots, its clear that the robust control law functions well and remains stable under varying free stream airflow conditions. All three targeted vibration modes have been reduced

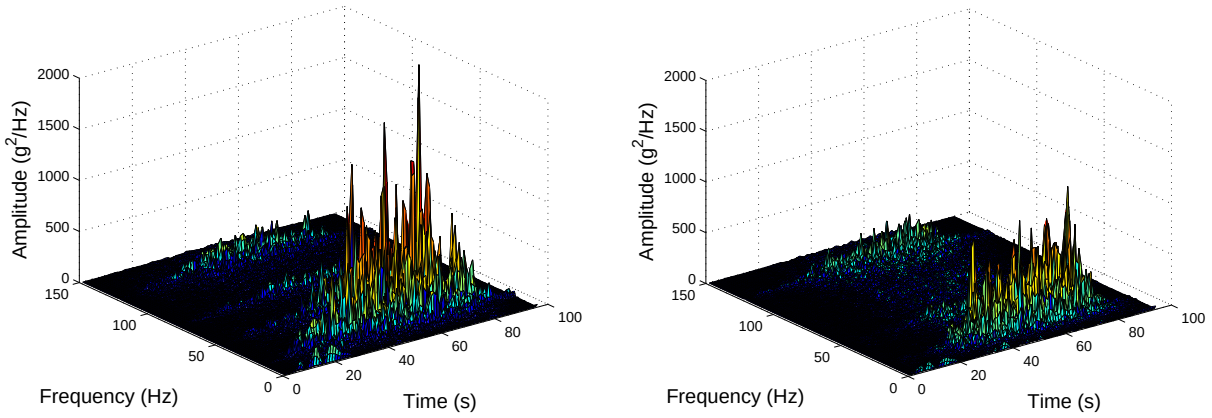


(a) Without Control

(b) With Control

**Figure 13. Robust Control Performance Under Variable Free Airflow Conditions**

significantly. On average, the first bending mode decreased by approximately $6.3dB$, the first torsional mode decreased by $4.4dB$ and the second bending mode decreased by $14.5dB$ throughout the variable free stream airflow test. Despite the wide range variation of airflow speed, the control law demonstrated satisfactory robust performance and provided significant load alleviation performance to the smart fin model.

## VI. Conclusion

Aeroelastic response of a scaled F-18 vertical fin was analyzed via wind tunnel experiments. It was observed that the frequencies and damping ratios especially at the torsion dominant modes vary according to flow condition. The extent of aerodynamic influence to the vertical fin dynamic properties increased with airflow speed and varied with orientation angle. Vertical tail buffeting loads were simulated using a vortex generator located upstream of the fin. The resulting aerodynamic loading was close to the fin's first bending mode. Mathematical models of smart fin were obtained without aerodynamic influence for different actuator settings. The $H_\infty$ controller problem was formulated considering the uncertainties in the estimated mathematical model, such as the unmodeled dynamics and parameter variations in the model due to aeroelastic coupling. Robustness analysis was performed for the designed controllers. The effectiveness and robustness of the control law has demonstrated through extensive closed-loop wind tunnel tests. It is shown that within the limited actuator capacity, robust controller design methods can provide fin buffeting alleviation.

## VII. Acknowledgement

This work was supported by NATO/RTA/Applied Vehicle Technology Panel through the project 'AVT/T-133 Development and Verification of Various Strategies for the Active Vibration Control of Smart Aerospace Structures Subjected to Aerodynamic Loading'. The authors gratefully acknowledge the support given.

## References

[1]Moses, R. W., "Vertical Tail Buffeting Alleviation Using Piezoelectric Actuators - Some Results of the Actively Controlled Response of Buffet-Affected Tails (ACROBAT) Program," *SPIEs 4 Annual Symposium on Smart Structures and Materials, Industrial and Commercial Applications of Smart Structures Technologies, Conference 3044, NASA Langley Research Center*, March 4-6 1997.

[2]F. Nitzsche, S. L. and Zimcik, D. G., "Theoretical and experimental investigations on an active control system for vertical fin buffeting alleviation using strain actuation," *The Aeronautical Journal*, Vol. 105, No. 2, 2001, pp. 277–285.

[3]F. Nitzsche, D. G. Zimcik, T. G. R. R. W. M. and Henderson, D. A., "Closed-loop control test for vertical fin buffeting alleviation using strain actuation," *Journal of Guidance, Control, and Dynamics*, Vol. 24, No. 4, 2001, pp. 855–857.

**Table 1. Variation of Smart Fin Modal Parameters Under Free Airflows**

| Air Flow Condition | | | First Bending | | First Torsion | | Second Bending | |
|---|---|---|---|---|---|---|---|---|
| | AoO ($deg$) | Air Speed ($m/s$) | Frequency ($Hz$) | Damping | Frequency ($Hz$) | Damping | Frequency ($Hz$) | Damping |
| Free Stream Air Flow Condition | 0 | 0 | 16.6 | 0.47% | 51.0 | 1.36% | 81.0 | 1.16% |
| | | 10 | 16.4 | 1.83% | 49.3 | 1.77% | 80.1 | 1.68% |
| | | 20 | 16.6 | 1.67% | 48.6 | 1.79% | 78.9 | 1.83% |
| | | 30 | 16.8 | 1.75% | 48.3 | 2.37% | 78.9 | 1.95% |
| | 10 | 10 | 16.6 | 2.90% | 48.9 | 1.73% | 77.9 | 1.58% |
| | | 20 | 16.3 | 6.10% | 47.7 | 1.86% | 76.6 | 1.86% |
| | | 30 | 16.1 | 6.52% | 47.6 | 2.91% | 76.4 | 2.32% |

**Table 2. Variation of Smart Fin Modal Parameters Under Vortical Flow**

| Air Flow Condition | | | First Bending | | First Torsion | | Second Bending | |
|---|---|---|---|---|---|---|---|---|
| | AoO ($deg$) | Air Speed ($m/s$) | Frequency ($Hz$) | Damping | Frequency ($Hz$) | Damping | Frequency ($Hz$) | Damping |
| Vortical Air Flow Condition | 0 | 0 | 16.6 | 0.47% | 51.0 | 1.36% | 81.0 | 1.16% |
| | | 10 | 16.6 | 2.00% | 48.1 | 1.77% | 77.4 | 1.30% |
| | | 13 | 16.6 | 2.31% | 48.6 | 1.80% | 77.9 | 1.42% |
| | | 15 | 16.6 | 2.42% | 49.3 | 1.78% | 77.5 | 1.53% |
| | 10 | 10 | 16.3 | 2.71% | 48.3 | 1.86% | 77.1 | 1.51% |
| | | 13 | 16.3 | 3.03% | 48.6 | 1.89% | 77.1 | 1.68% |
| | | 15 | 16.3 | 2.68% | 48.8 | 1.86% | 77.0 | 1.75% |

[4]Y. Chen, V. Wickramasinghe, D. G. Z., "Active Control of a Hybrid Actuation System for Aircraft Vertical Fin Buffet Load Alleviation," *Aeronautical Journal*, Vol. 110, No. 1107, 2006, pp. 315–326.

[5]Breitsamter, C. and Laschka, B., "Aerodynamic Active Control for EF-2000 Fin Buffet Load Alleviation," .

[6]S. Phillips, C. Lambert, I. G., "Effect of a Trailing-edge Jet on Fin Buffeting," *AIAA-2002-3065* $1^{st}$ *Flow Control Conference*, 24-26 June 2002.

[7]Caliskan, T., *Piezoelectric Ceramics And Their Applications in Smart Aerospace Structures*, Ph.D. thesis, Aerospace Engineering, Middle East Technical University, Turkey, 2002.

[8]Ulker, F. D., *Active Vibration Control of Smart Structure*, Master's thesis, MSc Thesis, Aerospace Engineering, Middle East Technical University, Turkey, 2003.

[9]M. Sahin, F. Karadal, Y. Y. O. F. K. V. N. F. D. U. T. C., "Smart Structures and Their Applications on Active Vibration Control:Studies in the Department of Aerospace Engineering, METU," *Journal of Electroceramics*, Vol. 20, 2008, pp. 167–174.

[10]Karadal, F. M., *Active Flutter Suppression of a Smart Fin*, Master's thesis, MSc Thesis, Aerospace Engineering, Middle East Technical University, Turkey, 2008.

[11]Dullerud G. D., P. F., *A course in Robust Control Theory*, Springer, 1999.

[12]Kemin Zhou, J. C. D., *Essentials of Robust Control*, Prentice Hall, 1998.